







Comparing the laser-induced damage distribution in POFs with raytracing simulations

KEVIN KIEDROWSKI,^{1,*}  MARIO FERRARO,^{2,3}  RAPHAEL JAUBERTEAU,²  STEFAN WABNITZ,²  MARIA CATERINA CROCCO,^{3,4} VINCENZO FORMOSO,^{3,4} MARCO JUPÉ,^{1,5} AND DETLEV RISTAU^{1,5,6}

¹Laser Zentrum Hannover e.V., Hollerithallee 8, 30419 Hannover, Germany

²Department of Information Engineering, Electronics and Telecommunications, Sapienza University of Rome, Via Eudossiana 18, 00184 Rome, Italy

³Department of Physics, University of Calabria, Via P. Bucci, 87069 Rende, Italy

⁴STAR Research Infrastructure, University of Calabria, Via Tito Flavio, 87036 Rende (CS), Italy

⁵Cluster of Excellence PhoenixD, Welfengarten 1A, 30167 Hannover, Germany

⁶Institute of Quantum Optics, Leibniz University Hannover, Welfengarten 1, 30167 Hannover, Germany

*k.kiedrowski@lzh.de

Abstract: The understanding of the laser-induced damage behavior in polymer optical materials is of high interest to prevent their damage and to increase the laser damage resistance of optical components. Moreover, compared with optical components made from high-quality glass materials, nanosecond laser-induced damage for wavelengths in the visible and near-infrared (NIR) occurs inside the bulk material of PMMA and not at its surface. This phenomenon complicates the determination of the laser-induced damage threshold (LIDT) in PMMA fibers. Since the bulk material itself determines the LIDT, knowledge of the intensity distribution in the multimode fiber is of utmost importance. Our fibers were irradiated at a wavelength of 532 nm with an ns-pulsed laser system with a 10 Hz repetition rate. To investigate the damage behavior in polymer optical fibers, we applied different imaging and analysis techniques. To our knowledge, those techniques are used here for the first time in order to study damaged polymer materials. With the help of a Nomarski microscope, axial and radial damage distributions within the multimode PMMA fibers were determined and compared with ray-tracing simulations of the intensity distribution within the optical fiber. Moreover, extruded PMMA plates were irradiated with the aim of comparing the damage behavior of materials with different manufacturing. In addition, the planar geometry of the plates allows for a more reliable application of the different measurement methods. Overall, investigations with a thermal imaging camera and EDX analysis indicate that the damage behavior of polymer optical material is thermally driven during the ns-pulsed irradiation. Furthermore, voids are formed during the damaging process within the polymer optical fibers and plates, as indicated by both SEM images and X-ray computed microtomography (μ -CT) investigations. Finally, we investigated the damages in fiber preforms and PMMA plates using two photon-microscopy. By doing this, we detected fluorescence signals from the damaged material, indicating that the damage process leads to a major modification of the polymer.

© 2024 Optica Publishing Group under the terms of the [Optica Open Access Publishing Agreement](#)

1. Introduction

In most cases, applications involving optical components are driven by both technological requirements and cost issues. This is particularly true when increasing the integration density of optical components and leads to reconsidering the use of low-cost materials that so far have been typically discarded for high performance applications. For this purpose, it is necessary to properly assess both the performance compatibility and the limited ranges of operation of

these materials. In this context, polymer optical materials have regained significant attention for their use in various applications. As a result, extensive scientific studies have been conducted in order to explore their range of usage, as well as to improve their properties. Specifically, when considering applications involving complex optical systems with high integration density, low-cost and easy-to-process polymers are seen as the future optical substrate materials of choice. Moreover, when compared to fused silica, polymers are lightweight and less expensive; moreover, the lower temperature during the manufacturing processes especially in case of optical fibers enables the integration of materials, e.g., nanocrystals and dyes, which otherwise would be damaged at higher temperatures. For example, recent detailed investigations involved polymer waveguides manufactured by flexographic printing [1], and a temperature measurement method based on nanocrystal doped polymer optical fibers which enables the temperature measurement in the vicinity of high electric fields [2]. Moreover, fiber sensor can be used in many areas of application by either intensity modulated or fiber Bragg grating based fibers, e.g. in the medical and structural health sector [3], realizing the measurement of humidity, temperature and strain [4]. Owing to the wide range of possible applications, and the accompanying increasing demand, the characteristics of polymer material behavior needs to be understood in full detail. One of the factors that limits the application of certain materials in the field of optics is the laser-induced damage threshold (LIDT). Laser-induced damages of different polymer materials were studied in detail in several investigations, with laser wavelengths ranging from 337 nm to 1064 nm and with different pulsed laser systems [5,6,7]. However, exact LIDT measurements of polymer optical fibers (POF) as the basic components for light guidance in future photonics applications are comparatively rare, even though the wave-guide properties and the manufacturing process might change the damage behavior drastically when compared with the unprocessed material. At variance with the case of optical glasses, laser-induced damages in polymer materials occur within the bulk material itself, under nanosecond pulse irradiation in the visible and NIR range. For example, an LIDT of 8.2 J/cm^2 measured for Poly(methyl methacrylate) (PMMA) when irradiated at a wavelength of 532 nm in the nanosecond pulse regime [8], ranges nearly one order of magnitude below the power handling capability of fused silica, which is around 60 J/cm^2 [8]. Nevertheless, owing to the specific advantage in many applications of using polymers as the optical fiber material, we performed detailed measurements of the damage behavior of PMMA fibers when irradiated with nanosecond pulses at a wavelength of 532 nm. The wavelength was chosen because Rhodamine B [9] as a possible doping for laser active POFs can be efficiently pumped at this wavelength. For this reason, these investigations serve as a preliminary study for doped fibers, which contain specifically implemented dyes acting as absorption centers. Moreover, due to the damage occurrence in the bulk of the polymer materials, the investigation of the damage distribution and its behavior is of high importance. This is because of the varying intensity distribution during beam propagation, which significantly impacts the damage distribution within a POF. In a previous study [10], we investigated the LIDT of POFs by performing long-term irradiation tests with pulse durations of 4.4 ns. The LIDT was determined to have a value of 50 mJ/cm^2 . However, improving the quality of polymer optical fibers requires the understanding of the damage behavior, and to gain information about the origin of the damage. For this reason, in this work we further analyzed the laser-induced damages that were earlier reported by using differential interference contrast (DIC) microscopy, in order to determine the damage distribution, and comparing it to the intensity distribution which is calculated by using a ray-tracing software. Additionally, to the best of our knowledge for the first time, we carried out both SEM and μ -CT measurements of POFs damaged by ns-pulses, in order to gain information about the damage morphology of our scanning laser optical tomography images [11]. Finally, by performing EDX analyses we have also investigated the element composition of the laser-induced material changes.

2. Simulated intensity distribution within a POF

In order to understand any damage behavior, it is necessary to have knowledge of the intensity distribution at the damage plane. However, the intensity distribution within a POF is rather complex, owing to the general total reflectance in the waveguide, and the possibility of inhomogeneities, which may change the incident beam profile. For this reason, we conducted ray-tracing simulations using the software OpticStudio by Ansys, Inc. [12], in order to investigate the change in the intensity distribution for the ideal case, meaning a perfect straight cylindrical rod.

The initial beam profile was set to a Gaussian, with a divergence similar to the experimental data, as described in the later section and a power of 1W was arbitrarily chosen. In addition, the refractive indexes of the core and cladding were 1.49 and 1.42 with diameters of 486 μm and 500 μm , respectively. The length of the fiber was set to 600 mm. The fiber length in the previously performed LIDT measurements was of 200 mm. Therefore, only two additional positions were considered for greater lengths. Furthermore, to simulate a more realistic measurement setup, the optical axis of the beam was misaligned by 0.5° , 1° or 3° degrees relative to the longitudinal axis of the fiber, respectively. In Fig. 1 the intensity distributions at different positions within the fiber cross sections are depicted for an input beam misalignment of 1° . The total energy in each cross section is nearly equal, as we neglect the presence of losses. However, the maximum intensity in each cross section differs, owing to the complex beam propagation. Therefore, the image intensity in each cross section was normalized with respect to its maximum value. The original Gaussian distribution is visible at the first position, right after the coupling of the light into the fiber at 0.1 mm. At 10–40 mm, the intensity distribution is already relatively inhomogeneous, owing to total reflection within the fiber. However, subsequent propagation within the fiber changes the intensity distribution even further: any statement concerning fiber homogeneity requires a detailed analysis of the corresponding images.

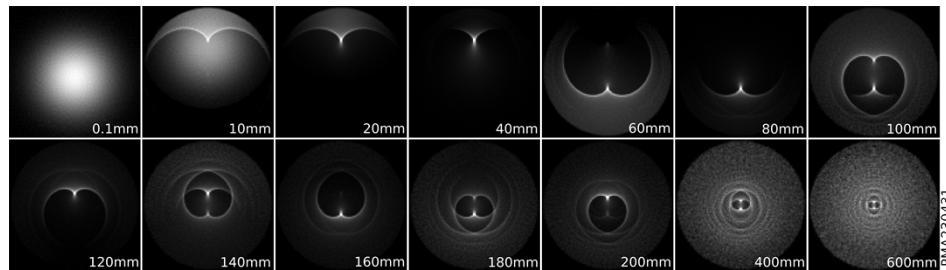


Fig. 1. Simulated images of the intensity distribution at specific fiber lengths using OpticStudios by Ansys, Inc.. A Gaussian beam was coupled into an optical fiber at an angle of 1° and for each position the grey scale is standardized to the maximum value.

In this case, we used the standard deviation of the beam transverse intensity profile as a mathematical quantity to describe the homogeneity of the light distribution within the fiber. A low standard deviation indicates that there is a rather homogeneous distribution of the laser beam within the fiber, whereby the relative intensities do not undergo abrupt changes. Whereas a high standard deviation is obtained in the presence of pronounced intensity peaks in the fibers cross-section. The corresponding computational results are plotted in Fig. 2.

Fig. 2 shows that, after the rapid initial increase, an overall decreasing standard deviation along the fiber is obtained, which indicates fewer and smaller peaks of the intensity distribution relative to the mean value, as expected from the images in Fig. 1. In addition, the larger the angle between the optical axis and the fiber longitudinal axis, the shorter the necessary propagation within the fiber to reach a high homogeneity of the intensity distribution. First of all, a bigger angle leads to a higher number of reflections at the core-cladding interface, resulting in a shift of

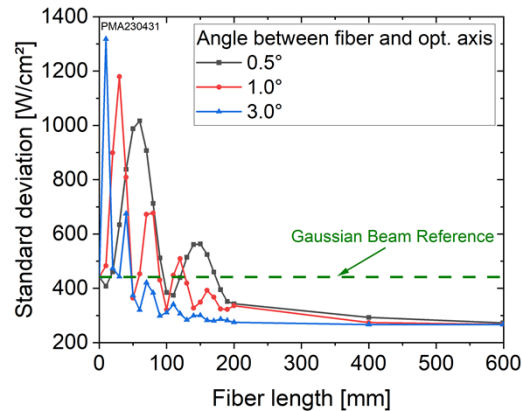


Fig. 2. The standard deviation of the simulated intensity distribution along the fiber for three different angles between the polymer optical fiber and the optical axis.

the local peaks of the periodic intensity fluctuation, which occur for smaller propagation lengths within the fiber. Secondly, due to the misalignment of the angle, propagation within the fiber is no longer rotationally symmetric. This leads to a ray distribution over a wider area for larger angles, which also creates a relatively fast intensity mixing within the fiber, ultimately leading to a more homogeneous intensity distribution over the fiber cross section. The change of the standard deviation for a three-degree misalignment angle and for a propagation length greater than 100 mm is very small, which shows that the intensity in the whole fiber cross-section is almost uniform.

During our previous investigations, we observed the occurrence of laser-induced damages in the core of the fiber, which is in good accordance with the general damage behavior observed in PMMA [5,6]. In addition, the damage process is defect-induced, owing to the presence of randomly dispersed inhomogeneities [6]. Based on this knowledge, it is possible to assume that material modifications within the fiber will occur at positions where the intensity distribution exceeds a certain threshold. To estimate the damage distribution along the fiber, we determined the number of pixels in the simulated images that exceed an arbitrary intensity threshold, and we standardized this sum of pixels' intensity to the total number of pixels in the fiber's cross-section. We repeated this procedure for different arbitrary intensity thresholds, representing higher or lower pulse energies coupled into the fiber at a fixed LIDT. The relative area of the fiber cross-section area where the intensity threshold is exceeded, as a function of the position in the fiber, is shown in Fig. 3 (a). Furthermore, we calculated the distance to the core center of each pixel which exceeds the threshold value. We then calculated the sum of the corresponding pixels in 20 μm wide intervals regarding the radial distance. The value was then normalized using the varying area of the related annuli with thicknesses of 20 μm . The resulting pixel density in dependence of the radial distance are depicted in Fig. 3 (b).

Overall, as one expects that the higher the pulse energy coupled into the fiber, the greater the relative area in the fiber cross section where the beam intensity exceeds the critical threshold. For relatively low pulse energies ($1 \cdot E_{\text{pulse}}$), the critical area shows a decreasing behavior along the propagation path in the fiber. This behavior can be explained in terms of the increasingly homogeneous intensity distribution along the fiber, as revealed by the corresponding low standard deviation in Fig. 2. Owing to the Gaussian beam profile in the first millimeters of the beam propagation, the critical intensity is only exceeded in the core center, that is within a small fraction of the core area. The propagation in the first 20 millimeters, up to the first total reflection, leads to a broader Gaussian beam, until a concentration of the beam energy on one side of the

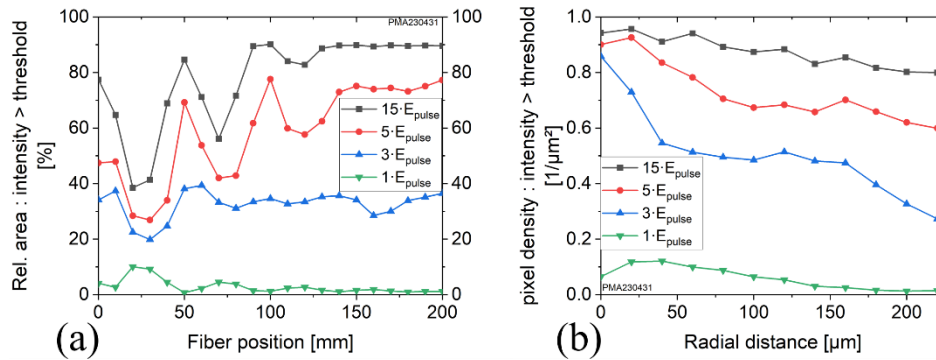


Fig. 3. Number of pixels that exceed a certain intensity threshold at the specified fiber position for an angle misalignment of 1° (a) and the sum of the pixels standardized to the corresponding annulus area with a thickness of $20\ \mu\text{m}$ versus the radial distance to the core center (b).

fiber occurs, due to the input misalignment. This leads to an increased proportion of the area where the intensity is below the critical threshold. However, further propagation along the fiber enhances the mixing of the beam modes so that only a few spots have an intensity in excess of the critical value. Consequently, an overall decrease of the above-threshold relative area is noticeable for low pulse energies. On the other hand, whenever high pulse energies ($5 \cdot E_{\text{pulse}}$ and $15 \cdot E_{\text{pulse}}$) are coupled into the fiber, the opposite behavior is observed. The high intensity of the Gaussian beam exceeds the threshold over a much wider area. However, the misalignment leads to a concentration of the beam energy at one side of the fiber, as seen in Fig. 1 (20 mm), leading to a decrease in the potentially endangered area. The subsequent uniformly distributed intensity along the propagation length leads to a very broad area in which the threshold is exceeded if the pulse energy is sufficiently high. Besides that, the two extreme cases of low and high pulse energies exhibit different behavior: for this reason, it is not surprising that a pulse energy ($3 \cdot E_{\text{pulse}}$) that lies in between the two previously described extreme cases leads to a rather constant value with distance of the total area where the intensity threshold is exceeded. The radial distribution shown in Fig. 3 (b) shows an almost consistent behavior with varying pulse energy. This graph indicates that a larger number of damages is expected the closer the specific area is to the core. However, for relatively high pulse energies, the homogeneously distributed intensity leads to an evenly distributed damage distribution within the polymer optical fiber.

Finally, it is important to note that the simulated data is based on an almost perfect setup, where only a misalignment angle is varied, in order to mimic the presence of the imperfections that occur in the experimental setup. However, impurities and imperfections inside a real fiber core, as well as in a partially rough core-cladding interface, lead to further scattering and the mixing of the beam intensity distribution during its propagation. Therefore, an even more evenly distributed intensity within the cross-section is expected in the experimental setup for any specific propagation length.

3. Laser-induced damages in polymer optical fibers

3.1. Measurement and determination of the LIDT

In a previous study, we investigated polymer optical fibers in detail regarding long-term [10] degradation under 4.4 ns-pulsed irradiation at a wavelength of 532 nm and a repetition rate of 10 Hz. The investigated fibers were not pre-annealed. In Fig. 4, we depict the measurement setup.

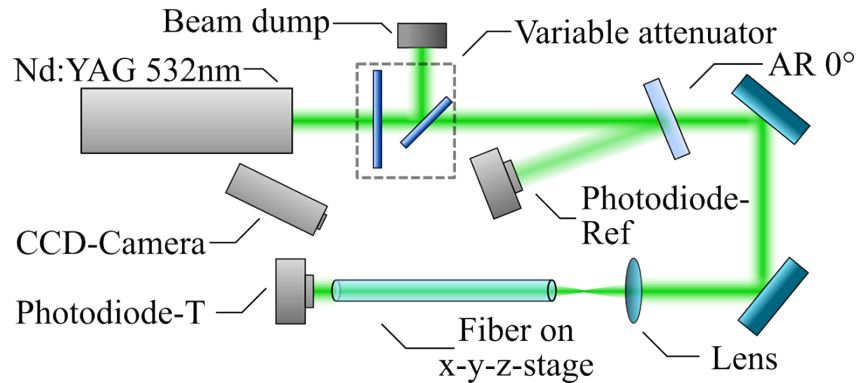


Fig. 4. Measurement setup for the determination of the laser-induced damage threshold.

The pulse energy of the irradiation was varied by a variable attenuator consisting of a half-wave plate and a polarizer. The laser beam was then focused by a lens, and the fiber was placed behind the focal spot so that most of the fiber core was illuminated without noticeable coupling losses. A CCD camera monitors the formation of scattering centers along the fiber, and a photodiode measuring the output energy of the fiber was used to monitor the transmission. A more detailed description of the setup is presented in our previous publication [10].

The long-term S-on-1 [13,14] study was conducted by coupling 40,000 pulses at a fixed pulse energy in POF. This was repeated for several pulse energies between 80 μJ and 1000 μJ . For each pulse energy, 5 to 7 fibers were tested. Overall, it has been shown that pulse energies above 80 μJ induce damages inside the POF, yielding a damage threshold of 80 μJ . Converted to an energy density, under the assumption that the intensity distribution is homogeneous in the fiber core with a diameter of 450 μm , the energy density amounts to 50 mJ/cm^2 . The fiber's losses are not included in the mentioned values because the damages occur at various positions along the fiber. Thus, a reliable determination of the pulse energies at specific positions is very difficult due to coupling losses in the range of approximately 5 to 6%, Fresnel losses, and the general fiber attenuation. Besides that, the fiber parameters used in the long-term study are listed in Table 1.

Table 1. Properties of the polymer optical fibers investigated in this work

Fiber length	200 mm
Diameter core/fiber	450 / 520 μm
Material core/cladding	PMMA / 404F acrylate
Refractive index core/cladding @ 852nm	1.49 / 1.40

3.2. Preparation and microscopy of the laser-induced damages

In this work, we studied the damaged fibers from the previous long-term study in order to investigate the damage distribution further, as well as the overall damage behavior in PMMA. To determine the axial and radial damage distribution, the fibers were investigated using a DIC microscope. For each pulse energy of the S-on-1 tests mentioned above, five fibers were inspected under the microscope. The fibers were placed between two coverslips filled with glycerin, which was used as an index-matching material to reduce refraction at the fiber due to its cylindrical form. Afterward, the fibers were positioned under the microscope and were investigated step-by-step in detail to count the laser-induced damages and to determine their corresponding axial and

radial position. When a damage was found, the fiber was rotated along the longitudinal axis to determine the radial position of the damage. The radial distance was measured by using the ZEISS microscope and the associated ZEN software. The axial distance relative to the fibers coupling facet was determined by using a manual length measuring tool. Overall, our inspection showed that damages predominantly occur in the volume of the fibers. As mentioned in a previous section, this is in good accordance with the general occurrence of laser-induced damages in the PMMA material [4,5].

3.3. Damage distribution in polymer optical fibers

First, by means of microscopy, we compared the relative degradation and the number of observed damages as a function of the pulse energy coupled into the fiber during LIDT measurements. The relative degradation is defined by the reduction in the fiber output signal compared to the initial output signal. The corresponding results are shown in Fig. 5.

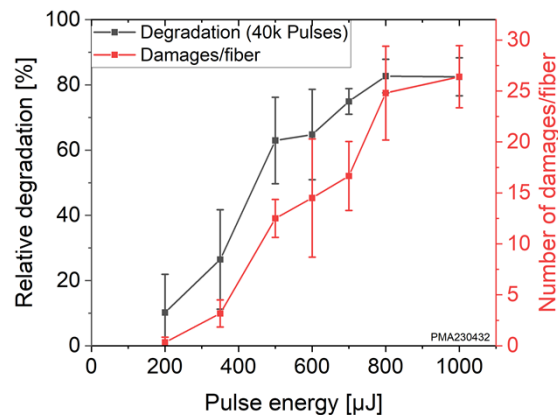


Fig. 5. Average relative degradation of polymer optical fibers after over 40.000 pulses, and average number of laser-induced damages due to irradiation, versus input pulse energy.

As expected, the number of laser-induced damages and the relative degradation increases with increasing pulse energy. The defects initiating the damage process have no discrete threshold but rather a threshold distribution, as proposed by various researchers investigating defect ensembles in different materials [13,14,15]. However, the damage behavior of polymers and especially POFs is very specific, and the behavior in Fig. 5 is in good accordance with our assumptions based on the simulations shown in Fig. 3. Independent of the radial or axial damage distribution, the potential area where laser-induced damages can occur increases with input pulse energy, leading to a greater total number of damages. Moreover, a strong correlation between the number of damages and the relative degradation is clearly visible in Fig. 5.

3.4. Axial and radial damage distribution within a polymer optical fiber

We evaluate the axial damage distribution within the fibers as a function of the corresponding input pulse energy (see Fig. 6). The axial damage distribution is defined by the damage position along the fiber longitudinal axis relative to the fiber front facet. The distribution at a relatively low pulse energy of 350 μJ shows a relatively high damage count within the first few centimeters of the fiber when compared with the damage counts at the fiber end. In the center and within the last few centimeters of the fiber, a decreasing number of damages is observed. However, for high pulse energy the number of damages seems to increase slightly with longer propagation in the fiber and approaches a saturated state. As mentioned above, we assume that the reason

behind the damage distribution is the intensity distribution within the fiber. In general, the intensity profile coupled into the optical fiber will change during the propagation due to the total internal reflection, as well as due to scattering at inhomogeneities within the core and the core-cladding interface. The intensity coupled into the fiber has a super-Gaussian distribution at the fiber entrance. However, during laser beam propagation, the intensity becomes progressively more homogeneous, as shown in the ray tracing simulations discussed in the previous section. Consequently, in most parts of the fiber cross-section, the energy density is below the LIDT, and a smaller number of damages are induced. All in all, the observed damage distribution for 350 μJ is in good accordance with our simulation for the case of relatively small pulse energies. For higher pulse energy, the homogeneous intensity distribution leads to a uniform increase of induced damages, because the pulse intensity lies above the LIDT over a larger area when compared with the first centimeters of the fiber, where the beam intensity is still super-Gaussian distributed. The reason for the observed damage distribution can be inferred from the discussion in the simulation section concerning the data of Fig. 3 (a). Overall, the cases for pulse energies of 800 μJ and 1000 μJ show an increase in the damage count along the fiber longitudinal axis, which is consistent with the simulation result for the relative area exceeding the critical threshold. Furthermore, a medium-to-high pulse energy of 500 μJ leads to a rather constant distribution, as expected from the simulated intensity distribution. It is important to note that for a 200 μJ pulse energy, only two damages were observed within the first 40 mm of the fiber.

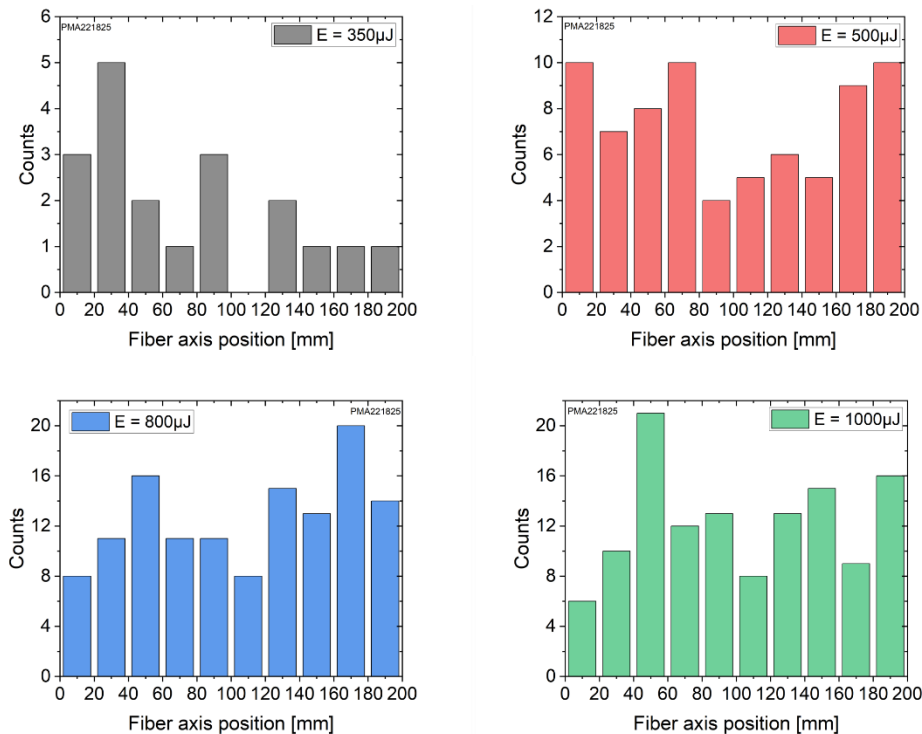


Fig. 6. Axial distribution of the laser-induced damages during long-term irradiation tests for different pulse energies.

In addition to the axial data, we also evaluated the radial damage distribution, which involves the distance of the damages relative to the center of the fiber. This was also carried out separately for different pulse energies. However, each bin of the histogram is defined by an annulus in the fiber cross-section with a width of 20 μm . The determined defect density is calculated from the

number of damages within the annulus, normalized by the corresponding annulus area. The damage density within each annulus for different pulse energies is presented in Fig. 7. For low energy densities, most of the laser-induced damages occur close to the center of the optical fiber, and are less than 50 μm away from the center. This is consistent with the previously described axial intensity distribution of the defects, which shows that at low pulse energies most damages are expected to occur within the first centimeters of the fiber (see Fig. 3). This is because, at the beginning of the propagation within the fiber, the laser beam intensity is still close to a super-Gaussian profile. Thus, the peak intensity is highest near the core center and decreases with increasing radial distance from the fiber axis, which limits the generation of a significant number of damages. Whereas, for high pulse energies the Gaussian distribution as well as the homogenous intensity distribution lead to laser-induced damages which are independent of the radial distance, as previously discussed in the simulation section. Therefore, the radial distance has no significant impact on the damage density for high pulse energies. The calculated pixel density exceeding a certain intensity threshold shown in Fig. 3 (b) indicates that there is an overall decrease of the damage density as the radial distance grows larger. However, this decrease is much larger at low pulse energies than at high pulse energies. In summary, simulations match well the experimentally observed trend of the damage density.

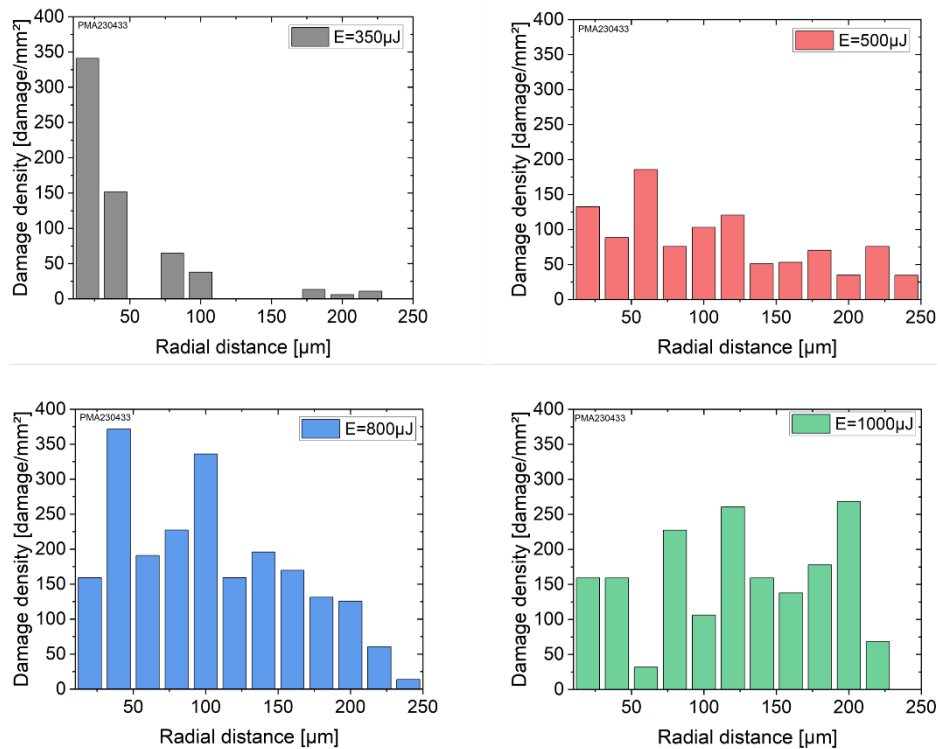


Fig. 7. Radial damage distribution of the laser-induced damages during the long-term irradiation tests for different pulse energies.

4. Morphology of laser-Induced damages in PMMA

In order to analyze the laser-induced damages further, detailed investigations of the induced damage morphology were carried out. A microscope image of damages in a PMMA preform and two images of the general dimension and shape of the damages in a POF are shown in

Fig. 8. Overall, damages in the fibers are similar to preform damages. The shapes are coarse, and stress-induced cracks occur. However, in the fiber the longitudinal axis of the elliptical damages is often oriented perpendicular to the fiber longitudinal axis, whereas in the preform no specific orientation is noticeable.



Fig. 8. DIC microscope image of laser-induced damages in the preform (a) and in the fiber core (b) and (c).

Overall, the information gained from DIC-microscope images is rather limited. For this reason, one may apply scanning laser optical tomography [11] in order to investigate the damage morphology. We searched for relatively large damage sites in the fiber core, cleaved the fiber with a ruby blade, and used a scanning electron microscope (SEM) to obtain high-resolution images (Fig. 9) of the damaged POF core. The observed damages are arbitrarily shaped voids in the PMMA core, and stress-induced cracks were noticeable in some images.

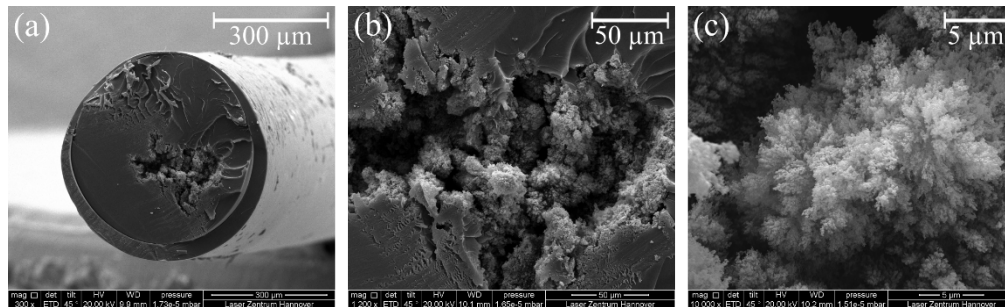


Fig. 9. SEM images of a laser-induced damage in the fiber core after the fiber was cleaved with a ruby blade. A magnification of 300 (a), 1,200 (b), and 10,000 (c) is used.

Along with the SEM images, we also conducted energy-dispersive X-ray spectroscopy (EDX) studies to further investigate the induced material change, and search for common contaminations [15] i.e., chromium, cobalt, iron, manganese, and copper in polymers. However, in neither area of the fiber core we found evidence of any of the mentioned contaminations. Therefore, we may conclude that either no contaminations are embedded in the core or the amount of the impurities is too low to be properly detected using EDX. Besides that, we analyzed the change in the material composition of two fibers (s. Figure 10). The amount of carbon is significantly higher in the damaged area than in the undamaged material. This indicates that the damage process is dominated by thermal mechanisms. A well-known process that might happen in PMMA due to pulsed laser irradiation in polymers is the thermolysis, which leads to carbonization, as discussed in detail by Butenin et al. [16,17]. This process leads to carbon and gas as byproducts. Moreover, a gaseous eruption might be visible in the image in Fig. 8 (c); and the material at the void's inner wall in Fig. 9 seems to be the result of high temperatures leading to a contraction and curling of the molecular chains. However, this only verifies that a thermal process happens during

laser irradiation with ns-pulses, but does not give direct information of the initiating process, for example owing to a high local absorption in the polymer volume or due to chain scission, etc.. Manenkov et al. [18] deduced from studies regarding the damage process of PMMA bulk material that the damage process is initiated by nanometer-sized impurities in the polymer matrix. Moreover, the literature discusses that the nanosecond pulsed irradiation of small particles in the polymer matrix can lead to high particle temperatures [16]. Subsequently, either thermal stress induces cracks in the polymer [19] or the particles, which are heated up to temperatures of several thousand degree, act like blackbodies emitting UV irradiation thus preionizing the material [18] leading to higher absorption. The results of the studies are well summarized in more detail by Fouassier and Rabek [6]. Besides that, it might also be possible that the emitted UV light directly damages the macromolecules, possibly leading to chain scission and degradation of the polymer. The degree to which the damage process is comparable to the production of fiber Bragg grids cannot be precisely determined by us in this study [4]. Furthermore, it is difficult to estimate whether pre-annealing of the POFs increases or reduces the LIDT. Higher temperatures might lead to relaxation, thus reducing possible inhomogeneities. However, it might also induce thermal stress between the present defects and the polymer matrix, favoring the laser-induced damage process.

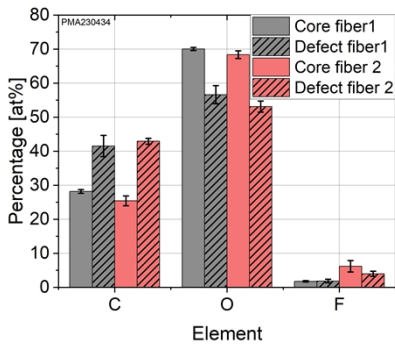


Fig. 10. EDX analysis of two fiber cross sections. In each fiber the element composition of an undamaged and a damaged area was investigated.

In order to further analyze the damage morphology, position, and size in PMMA optical fibers, we employed X-Ray μ -CT. This experiment was based on the recently proposed μ -CT study of glass optical fibers by Sandoghchi et al. [20]. The technique consists of exploiting the different X-ray absorption properties, which are related to the difference in material density of the fiber core and cladding, respectively. This permits the three-dimensional morphology of the sample to be revealed. Given that the material density is related to the material refractive index, μ -CT can be used as a tool for obtaining a 3D-map of the refractive index of the fiber core [21]. Remarkably, this has also permitted to spot the presence of damages and defects of standard silica optical fibers which appear as a local variation of the material density [22].

Our results obtained on a 1.2 cm long fiber span are reported in Fig. 11. The spatial resolution of our setup is about 5 μ m in all directions. Figure 11(a) shows the 3D reconstruction of the POF. The image on top of the panel is the bare reconstruction of the fiber. In the image right below, we increased the transparency of the colors, in order to highlight the presence of a damage (red zone inside the fiber volume). The damage is even more evident in the image at the bottom of Fig. 11(a), where we applied a thresholding filter on the intensity scale. Specifically, the damaged volume has a non-spherical shape (the computed sphericity was 0.65) with a width of 39 μ m and a length of 73 μ m.

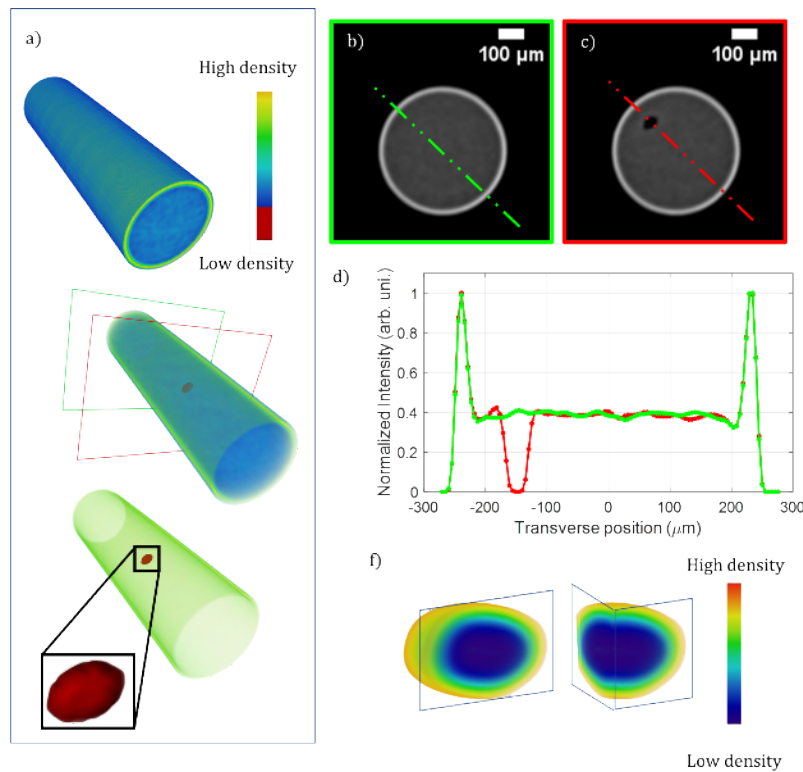


Fig. 11. (a) 3D rendering of the optical fiber within different visualizations: bare tomographic reconstruction (top); transparency-enhanced visualization (middle); after applying a thresholding filter in order to emphasize the damage (bottom), which is shown in the inset; (b,c) Slices of tomographic reconstruction along the cutting planes in (a): the red and the green boxes show the inner part of the PMMA fiber with and without damage, respectively; (d) intensity profile traces corresponding to the dot-dashed lines in (b,c); (e) zoom of 3D reconstruction around the damage.

In Fig. 11 (b) and (c) we show two transverse slices of the tomographic image at different longitudinal positions (see the color correspondence with the middle image of Fig. 11 (a)). Specifically, the slice in Fig. 11 (c) crosses the damage, whereas that in Fig. 11(b) is associated with a position that is far away from the damage. The intensity profiles along the dot-dashed lines in Fig. 11 (b) and (c) are reported in Fig. 11 (d). As can be seen, the red and green curves perfectly overlap, except for the damaged region. In particular, one may notice that the red curve reaches a minimum, whose value is close to zero, which corresponds to a reduction of material local density. Especially, a value of μ -CT close to 0 indicates that a void is formed, in agreement with the observations in Fig. 9.

On the contrary, at the edges of the damage, the density increases, as indicated by the local maximum of the red curve. Such a spatial density redistribution is better highlighted in Fig. 11 (e), where we zoomed in the 3D reconstruction around the damage (note that the color scale is different from that of Fig. 11 (a)). We report two different cuts of the damage in order to emphasize the spatial distribution of the material density. Such a μ -CT intensity indicates that an increase in the material density occurs at the edges of the damage, consistently with the principle of mass conservation. Furthermore, owing to the damage process, stress might be induced and frozen in this area. However, we should emphasize that, when dealing with edges,

the equivalence between the μ -CT intensity and the material density is not fully reliable because of the occurrence of edge-enhancement effects [21].

5. Material study on PMMA-plates

In order to narrow down the possible number of damage initiators, it is necessary to carry out detailed analysis of the damage morphology. However, the geometry of the POFs makes the damage investigation particularly challenging. For this reason, we also irradiated commercially available extruded PMMA plates with a size of $100 \times 100 \times 2 \text{ mm}^3$ with a nanosecond pulsed laser system at a wavelength of 532 nm and a 100 Hz repetition rate. An S-on-1 measurement [13,14] with 6000 pulses per position was performed, yielding a LIDT of 40 mJ/cm^2 for the extruded PMMA plates. This value is in good agreement with the results obtained for the POFs, but it is lower than the PMMA waveplate LIDT of 0.46 J/cm^2 that was determined by Melninkaitis et al. [5], and the preform LIDT of 0.57 J/cm^2 that was measured by us. Such a deviation may be attributed to the higher repetition rate and the larger pulse number that we used in the present work. It might also be related to a different grade of the PMMA plate, but our results suggest that this only results in a reduced LIDT or a higher number of damaged spots. However, the damage mechanism is most likely comparable. The aim of the irradiation was to generate damages in a large area in order to ease the investigation with subsequent measurement setups. During the irradiation, a high-resolution microscope was used to monitor the damage growth in the laser spot area, and an infrared camera was employed for the inspection of the temperature increase in the area of interest. Three images of a recorded movie taken with the online microscope during an irradiation sequence of a single spot with up to 40.000 pulses are shown in Fig. 12.

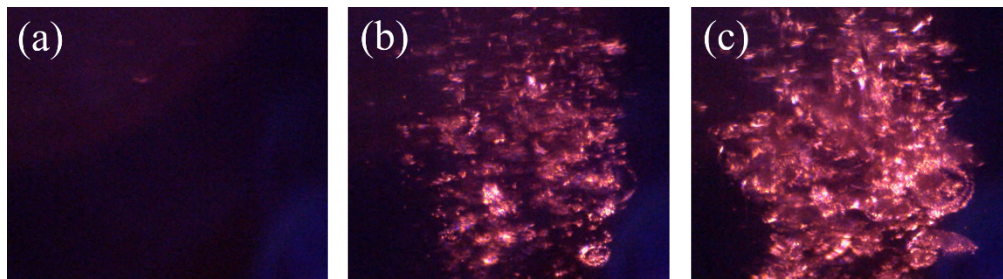


Fig. 12. Damage growth during laser irradiation with a laser diameter of 2 mm ($1/e^2$) after approximately 0 (a), 2.600 (b) and 40.000 (c) pulses.

During the irradiation, we observed light scattered by the laser-induced damages. Over time, the number of scattering centers increases; with an increasing number of pulses, the induced damages grow in size, as seen in image (c). Afterwards, the irradiated spot shown in Fig. 12 was investigated with a high-resolution microscope. An image of the same spot and of another spot irradiated with only up to 6.000 pulses at the same energy density were taken using a DIC microscope. These images are shown in Fig. 13 to demonstrate the damage morphology at different stages. A similar damage growth behavior was observed in the POFs by using a CCD camera.

Moreover, the dimension and shape of the damages are similar to the damages that we observed in POF. Randomly dispersed and coarse damages occur in the irradiated area, and sometimes cracks are induced by stress. Specifically, the higher pulse numbers lead to larger damages.

As previously discussed, the EDX analysis of damage in the POF core indicates a thermal origin of damages, which is associated with an increase of carbon as a product of thermolysis. For this reason, we used an infrared camera to verify if an increased temperature can be detected during the irradiation with a pulse width of 6 ns and a 100 Hz repetition rate. The infrared camera

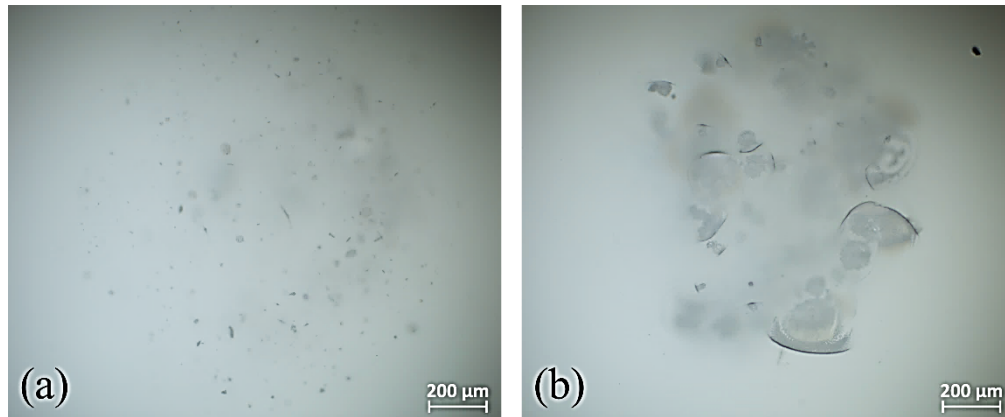


Fig. 13. Damage growth in a PMMA plate during laser irradiation with a laser diameter of 2 mm ($1/e^2$) after approximately 6.000 (a) and 40.000 (b) pulses.

was not calibrated to the emissivity of the material, but the irradiation of 3000 pulses with an energy density of 2.5 J/cm^2 , as depicted in Fig. 14 (a) led to a relative temperature increase of approximately $20 \text{ }^\circ\text{C}$. It is reasonable to assume that the local temperature at the absorbing defects is significantly higher. Moreover, laser-induced damages in a fiber preform and in a PMMA plate were investigated by using 2-photon microscopy pumped by a fs-laser at 1030 nm (Fig. 14 (b) and (c)). Using this technique, only the damaged material shows fluorescence, which indicates that the laser-induced material modification leads to significant changes in the chemical structure of the polymer. Moreover, the size of the damages is only a few micrometers, and we did not observe any fluorescence in a non-irradiated reference area. As a result, most likely, the randomly distributed initiators within the PMMA that lead to the damage are nanometer-sized. Thus, they are not resolvable with optical methods. This is in good agreement with the results of several studies reported in the literature [6,16,18] as already discussed in section 4.

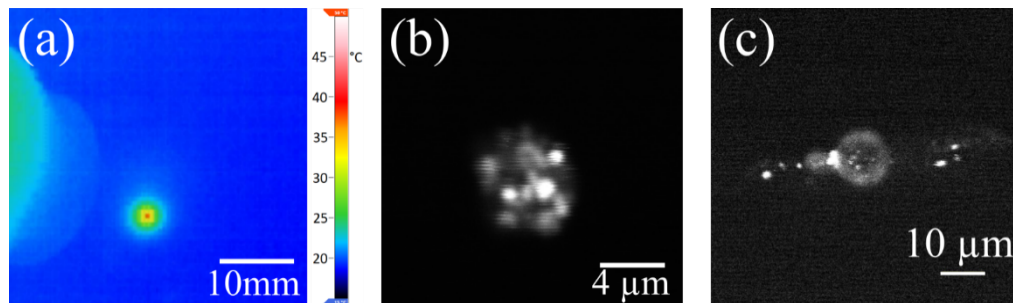


Fig. 14. (a) Image of the infrared camera showing the heating of the PMMA plate due to the laser radiation after approximately 3.000 pulses at a repetition rate of 100 Hz, a wavelength of 532 nm, a pulse duration of 7.3 ns and an energy density of 2.5 J/cm^2 . The online microscope is visible on the left side. (b) Laser-induced damage in a PMMA fiber preform and (c) in a PMMA plate visualized by the fluorescence using 2-photon microscopy.

6. Conclusion

We conducted in-depth investigations of the laser-induced damage behavior within POF, showing that the damage distribution depends strongly on the intensity distribution of the laser beam

inside the fiber. Moreover, the damages are driven by the presence of defects in the fiber material. The observed distribution of material modification inside the POF was determined by using a DIC microscope, and it was shown to be in good accordance with the intensity distribution that we simulated with a ray tracing software. Our study shows that the properties of laser-induced damages in POF are consistent with the literature on damages in polymer materials, and are governed by the presence of randomly distributed defects in the bulk material. However, the complex and changing intensity distribution within the optical fiber needs to be considered when estimating the LIDT in POF. The data gained from our study also indicates that laser irradiation coupled into the fiber should be as homogenous as possible in order to distribute the intensity across the whole fiber core, thus reducing local intensity maxima. Especially, with regard to laser-active fibers with dopants further promoting damages due to local absorptions, a homogenous intensity distribution would minimize the risk of inducing damages. In doped POFs, we expect the damage to happen at the implemented nanocrystals or dyes due to the increased absorption. Furthermore, the study shows that laser-induced material modifications occur preferentially at randomly distributed defects within the fiber core. This might also have an impact on the manufacturing quality of fiber Bragg gratings depending on whether a defect is illuminated or not.

Furthermore, we investigated the damage morphology by X-ray computed microtomography of POF. The results of this study are in good accordance with SEM images, and provide additional information on the material density without the need for a special preparation of the damaged area, e.g., without the need to cleave the fiber. The analysis of damages formed during laser irradiation shows the presence of a void with slightly increased material density at the edges. This reveals a space-consuming damage process and leads us to presume that stress may be induced and frozen in the damaged area. Additionally, the presence of thermolysis was indicated by both an IR camera and EDX, which is in accordance with literature results. Moreover, material modifications were visualized not only with μ -CT and SEM analyses but also by 2-photon fluorescence signals from the modified area. This indicates a change of the refractive index, which additionally to the induced voids, can lead to scatter losses limiting the functionality of the fiber.

To conclude, on the one hand our work verifies that the damage mechanism in POF is driven by the presence of randomly distributed defects, hence it strongly depends on the intensity distribution within the optical fiber. On the other hand, we introduced different promising approaches for the in-depth analysis of laser-induced damages in POF, which permitted us to gain information on the damage morphology and the material modifications.

Our investigations of laser-induced damages suggest that PMMA is only suitable for comparatively low performance applications due to the low laser-induced damage threshold compared to other glasses. Nevertheless, the presented study can be considered as a reference for the investigation of bulk destruction of fibers and other solids with complex geometries in which laser-induced damages occur in the volume. Our analysis shows that, even in the case of complex beam propagation in a bulk material, statistical correlations between the simulated intensity distribution and the position of laser-induced damages can be obtained. Thus, it can be estimated whether a defect-driven damage will be induced or not. Additionally, critical areas in which a high energy density is expected can be monitored in more detail. Moreover, we have shown that high-resolution and innovative methods allow for a much deeper insight into the destruction processes than DIC microscopy. In perspective, additional investigations deserve to be carried using the presented methods for the study of alternative polymers or inorganic materials.

Funding. Ministero dell'Istruzione, dell'Università e della Ricerca (PIR01-00008, R18SPB8227); NextGenerationEU, partnership on "Telecommunications of the Future" (PE00000001 - program "RESTART"); Deutsche Forschungsgemeinschaft (EXC2122, Project ID 390833453); European Regional Development (LAPOF (contract no. ZW 685003502)).

Disclosures. The authors declare no conflicts of interest.

Data availability. Data underlying the results presented in this paper are not publicly available at this time but may be obtained from the authors upon reasonable request.

References

1. A. Evertz, G.-A. Hoffmann, E. Olsen, *et al.*, “Industrial processing for printed polymer optical waveguides,” *Proc. SPIE* **11815**, 10 (2021).
2. J. Thiem, S. Spelthann, L. Neumann, *et al.*, “Upconversion nanocrystal doped polymer fiber thermometer,” *Sensors* **20**(21), 6048 (2020).
3. C. A. F. Marques, D. J. Webb, and P. Andre, “Polymer optical fiber sensors in human life safety,” *Opt. Fiber Technol.* **36**, 144–154 (2017).
4. R. Oliveira, L. Bilro, and R. Nogueira, *Polymer Optical Fiber Bragg Gratings: Fabrication and Sensing Applications* (CRC Press, 2019).
5. A. Melninkaitis, D. Mikšys, M. Maciulevičius, *et al.*, “Laser-induced damage thresholds of starched PMMA waveplates,” *Proc. SPIE* **6403**, 640325 (2006).
6. J. P. Fouassier and J. F. Rabek, *Lasers in Polymer Science and Technology: Applications, Volume IV* (CRC Press, 1989).
7. R. Wandschneider, K.-F. Klein, and G. Hillrichs, “Transmission properties of polymer optical fibers for pulsed UV,” *Proc. SPIE* 6852, SPIE BiOS., San Jose, California, United States (2008).
8. H. Gebauer, M. Jupé, D. Ristau, *et al.*, “Measurement of laser power resistance of fibers for PIV systems,” *Laser-Induced Damage in Optical Materials* **7132**, 713219 (2008).
9. S. Spelthann, S. Unland, J. Thiem, *et al.*, “Towards highly efficient polymer fiber laser sources for integrated photonic sensors,” *Sensors* **20**(15), 4086 (2020).
10. K. Kiedrowski, F. Jakobs, J. Kielhorn, *et al.*, “Laser-induced degradation and damage morphology in polymer optical fibers,” *Proc. SPIE, SPIE Photonics Europe* **11355**, 1135504 (2020).
11. K. Kiedrowski, J. Thiem, F. Jakobs, *et al.*, “Determination of the laser-induced damage threshold of polymer optical fibers,” *Proc. SPIE* 10805, *Laser-Induced Damage in Optical Materials*, (2018).
12. Ansys Inc. <https://www.ansys.com/products/optics-vr/ansys-zemax-opticstudio>, (30.11.2023).
13. International Organization for Standardization, “DIN EN ISO 21254-1:2011-10, Laser und Laseranlagen - Prüfverfahren für die laserinduzierte Zerstörschwelle - Teil 1: Begriffe und allgemeine Grundsätze”, Beuth Verlag, (2011).
14. International Organization for Standardization, “DIN EN ISO 21254-2:2011-10, Laser und Laseranlagen - Prüfverfahren für die laserinduzierte Zerstörschwelle - Teil 2: Bestimmung der Zerstörschwelle”, Beuth Verlag, (2011).
15. J. Zubia and J. Arrue, “Plastic optical fibers: an introduction to their technological processes and applications,” *Opt. Fiber Technol.* **7**(2), 101–140 (2001).
16. A. V. Butenin and B. Y. Kogan, “Mechanism of damage of transparent polymer materials due to multiple exposure to laser radiation pulses,” *Soviet Journal of Quantum Electronics* **5**(6), 611–613 (1976).
17. A. V. Butenin and B. Y. Kogan, “Mechanism of laser damage to polymer materials,” *Soviet Journal of Quantum Electronics* **16**(10), (1986).
18. A. A. Manenkov and V. S. Nechitaïlo, “Role of absorbing defects in laser damage to transparent polymers,” *Sov. J. Quantum Electron.* **10**(3), 347–349 (1980).
19. M. I. Aldoshin, B. G. Gerasimov, A. A. Manenkov, *et al.*, “Decisive importance of the viscoelastic properties of polymers in their laser damage mechanism,” *Sov. J. Quantum Electron.* **9**(9), 1102–1105 (1979).
20. S. R. Sandoghchi, G. T. Jasion, N. V. Wheeler, *et al.*, “X-ray tomography for structural analysis of microstructured and multimaterial optical fibers and preforms,” *Opt. Express* **22**(21), 26181–26192 (2014).
21. M. Ferraro, M. C. Crocco, F. Mangini, *et al.*, “X-ray computed μ -tomography for the characterization of optical fibers,” *Opt. Mater. Express* **12**(11), 4210–4222 (2022).
22. M. Ferraro, F. Mangini, Y. Sun, *et al.*, “Multiphoton ionization of standard optical fibers,” *Photonics Res.* **10**(6), 1394–1400 (2022).